Measurement of shock pressure and shock-wave attenuation near a blast hole in rock

Li Yuan Chi , Zong Xian Zhang , Arne Aalberg , Jun Yang , Charlie C. Li

PII: S0734-743X(18)30638-9
DOI: https://doi.org/10.1016/j.ijimpeng.2018.11.002
Reference: IE 3195

To appear in: *International Journal of Impact Engineering*

Received date: 26 June 2018
Revised date: 16 October 2018
Accepted date: 7 November 2018

Please cite this article as: Li Yuan Chi , Zong Xian Zhang , Arne Aalberg , Jun Yang , Charlie C. Li , Measurement of shock pressure and shock-wave attenuation near a blast hole in rock, *International Journal of Impact Engineering* (2018), doi: https://doi.org/10.1016/j.ijimpeng.2018.11.002

Highlights

- Granite cylinders with a central charge were blasted
- Shock pressures were measured at distances 7-35mm from borehole
- Peak pressures varied from 15.9-4.4 GPa depending on the distance
- Near-field shock-wave velocities depended strongly on the distance
- Shock-wave attenuation with distance can be approximated by an exponential relation

Measurement of shock pressure and shock-wave attenuation near a blast hole in rock

Li Yuan Chi [a, b,*]; Zong Xian Zhang [c]; Arne Aalberg [a]; Jun Yang [d]; Charlie C. Li [b]

[a] Department of Arctic Technology, the University Centre in Svalbard (UNIS), Longyearbyen, Norway;

[b] Department of Geoscience and Petroleum, Norwegian University of Science and Technology (NTNU), Trondheim, Norway;

[c] Oulu Mining School, University of Oulu, Oulu, Finland;

[d] State Key Laboratory of Explosion Science and Technology, Beijing Institute of Technology, Beijing, China.

* Corresponding author
Email address: liyuan.chi@unis.no (L.Y. Chi)

Abstract

The objective of this study was to investigate granite responses to blasting. The focus was on the pressure and attenuation of shock waves in granite. Tests are reported on ten cylinders subjected to explosions from central pressed trinitrotoluene (TNT) charges with approximate density of 1.6 g/cm^3. Three cylinders had dimensions Ø150 mm × 200 mm; seven, Ø240 mm × 300 mm. Specimens had concentric holes drilled from both ends: one 20-mm hole to position the explosive charge and one 50-mm hole to insert a granite plug equipped with Manganin gauges, which were applied to monitor the pressures of the shock waves. The configuration of the gauges was analyzed before testing to investigate how precisely they could measure shock waves in the granite. One or two gauges were used in each cylinder at distances of 7, 15, 22 or 35 mm from the explosive charge in the cylinder axis. At detonation of the charge, the measured peak pressure values ranged from 15.9–4.4 GPa depending on distance from the explosive, with pressure rise times of ~0.5 μs. In one specimen, deflagration occurred, resulting in a low peak pressure of 1.35 GPa 11 mm from the explosive and a 16-μs pressure rise time. For specimens with two gauges, shock-wave velocities were found to depend strongly on the distance from the explosive. Fitting a curve to the experimental data, an exponential relation for the shock-wave peak pressure and its attenuation was obtained, expressing pressure (GPa) as a function of increasing distance (mm) from the explosive: $p = 19.4\exp(-0.04x)$. The findings, especially regarding the damping term, may for instance be useful for verification of numerical models for blasting simulation.

Keywords: blast experiment, granite cylinder, Manganin pressure gauges, shock compression

1. Introduction

Rock blasting plays an extremely important role in hard rock mining and other rock engineering works. Until now, rock blasting has been dominated by empirical design, which, to a varying extent, may result in mineral loss, poor safety and a waste of explosive energy. An improved and scientifically based blast design will depend on a better understanding of the fundamentals of rock blasting, which include detonation physics, shock-wave characteristics, rock fracturing and fragment movements. The shock compression of the rock in the vicinity of an exploding charge is of particular importance, as this compression is associated with high energy consumption and strongly influences the stress waves generated in the rock, which in turn initiate dynamic fractures in the far field and subsequent rock fragmentation. In this context, proper measurements of detonation-caused shock pressure and shock-wave attenuation in rock are particularly important.

Since the 1980s, several scientists have attempted to measure the shock pressures occurring in blasting. Some results from the limited previous studies are summarized here, revealing large variations. Fourney et al. [1,2] measured the borehole pressure under the stemming in polymethyl methacrylate (PMMA) block specimens and found that the maximum pressures were of the order of magnitude of 10 MPa in highly decoupled blastholes. Nie [3] measured the borehole pressure in large granite blocks by using carbon resistor gauges and found maximum pressures typically varying from 0.08 GPa to 1.4 GPa. Mencacci and Chavez [4] measured the pressures in boreholes in an open pit mine and found that the maximum pressures were higher than 8 GPa in fully charged boreholes loaded with ammonium nitrate/fuel oil (ANFO). Banadaki and Mohanty [5] measured point pressures in granite specimens at 11 mm to 45 mm from the boreholes loaded with small charges (approximately 0.45 g pentaerythritol tetranitrate, PETN) and found that the maximum pressures were approximately 70 MPa. Davies et al. [6] used polyvinylidene fluoride (PVDF)

gauges to obtain the stresses in polytetrafluoroethylene (PTFE) blocks inserted in boreholes and found maximum compressive stresses ranging from 6.1 GPa to 14.8 GPa. Taylor et al. [7] used similar gauges in limestone and measured maximum stresses of approximately 3.5 MPa at a distance of 200 mm from the borehole.

Different pressure gauges have different characteristics in shock pressure measurements. Ginsberg & Asay [8] noted that carbon resistor gauges had better survivability than did Manganin gauges in some applications and recommended that carbon resistor gauges (470 Ω) be used to measure pressures up to 5 GPa. Rosenberg et al. [9] performed plate impact experiments and found that carbon resistor gauges were not capable of capturing data for rise times shorter than 0.5 μs due to response time considerations. Moreover, these authors noted that the resistive hysteresis in carbon resistor gauges upon stress unloading is not clear. The descending part of the pressure signal may therefore not be captured accurately with such gauges. Davies et al. [6] and Bourne [10] commented that the manufacturing reproducibility of PVDF gauges significantly influences their accuracy; thus, the gauges require calibration by impact experiments. In addition, the cost of PVDF gauges is much higher than that of piezoresistive gauges (e.g., Manganin and carbon resistor gauges). For Manganin gauges, the resistance change is insensitive to the surrounding temperature [10], and the gauge failure at high pressures (60 GPa) is due to the phase transition in the polymer part of the gauge that occurs at the high temperature caused by the shock wave [11]. The characteristics give Manganin gauges an advantage in shock pressure measurement if a rise in temperature is possible.

Shock pressure measurements in rock have also been conducted by employing plate impact experiments, in which a step input of pressure is generated to simulate the shock loading in rock blasting [12–15]. However, for attenuation of the shock wave in rock materials, only a limited number of investigations have been performed to date. Haas et al. [16] used the pellet

technique to investigate the attenuation of shock wave in marble plates and found peak stresses of approximately 1.9 GPa at a distance of 13 mm from the impacted surface and 0.1 GPa at a distance of 102 mm. The attenuation of the shock wave is directly related to the release state. Petersen et al. [17] measured the particle velocity to obtain the release-adiabat curves for alluvium and found that an initial release wave velocity equal to two times that of the shock front caused a rapid attenuation of the shock wave. Applying pressure gauges embedded in the specimens in plate impact experiments, Nakazawa et al. [18] investigated shock-wave attenuation in basalt. The measured shock-wave pressures were approximately 7 GPa in the far field, which was more than 15 mm from the impacted surface according to their definition, where the attenuation was found to depend on the propagation distance raised to the power of -1.7 to -1.8. Tilert et al. [19] studied granite blocks subjected to explosions from charges (1 g, PETN) in drilled holes and investigated block thickness limits where spalling starts to occur and how a crack in the granite attenuated the shock-wave amplitude.

The aim of the present study was to perform precise measurements on the shock pressure and shock-wave attenuation in granite near blast holes. Foil Manganin gauges were located at positions along the specimen axis at different distances from the explosives. The experiments were designed with the intention of obtaining a better basic understanding of the shock-wave characteristics and the developed experimental data may be used for validating numerical tools such as models developed to simulate rock blasting or detonation [20–22].

2 Rock material and experimental method

2.1 Rock material

Cylindrical rock specimens manufactured from granite from Fangshan (Beijing, China) were used in this investigation. The material properties were determined by performing both static and dynamic tests, as presented in Chi et al. [23]. The granite had a density of 2.74 g/cm^3, a

Poisson's ratio of 0.23, a uniaxial static compressive strength of 84.1 MPa, a static tensile strength of 6.3 MPa and a compressive strength of 130 MPa at a strain rate of 90 /s. According to the supplier, the longitudinal wave velocity in the granite varies between 4000 m/s and 4400 m/s. The major geochemical components of the granite were SiO_2 (33.6-56.9 wt%), MgO (5.3-9.4 wt%), and CaO (1.5-14.8 wt%). The dominant heavy mineral was magnetite (1.01 wt%) with grain sizes up to 0.7 mm. The grain sizes of the other heavy minerals were in the range of 0.05-1.1 mm.

2.2 Test setup

The blasting experiments were conducted in an explosion chamber at the Beijing Institute of Technology. The chamber consists of a closed explosion room with an inspection window. The details of the test arrangements are given in Chi et al. [23]. The rock specimens (Fig. 1) were placed on granite support blocks in the chamber, and the blasting process was monitored using a high-speed camera. To measure the shock pressure and to investigate the shock attenuation, Manganin gauges were embedded in the specimens. Either one or two gauges were used in each specimen. The Manganin gauges required a DC power supply and a quarter Wheatstone bridge for signal conditioning. A 24-bit isolation data acquisition device (LTT24, LTT Labortechnik Tasler GmbH) with an integrated signal conditioning module was used to record the pressure signals. The sampling frequency was set to 4 MHz, and the corresponding dynamic range of the recording module was 94 dB. In addition, the maximum bandwidth was 1.7 MHz, which means that signals with a bandwidth greater than 1.7 MHz could not be precisely captured. To synchronize the data acquisition instrument with the detonator, an enamel insulated wire was placed between the detonator and the explosive charge [23]. The length and diameter of the detonator were 50 mm and 7 mm, respectively (Fig. 2).

2.3 Pretests and pressure gauge placement

Shock pressure in rock is commonly measured either in the radial or axial direction of a blast hole. In this study, five pretests on granite cylinders were performed to select the most appropriate pressure gauge placement and charge parameters. All pretest specimens had a pressure gauge positioned at a distance of 10 mm from the bottom of the charge, with its pressure-sensitive plane oriented perpendicular to the shock-wave direction. In three of the specimens, an additional pressure gauge was applied in order to monitor the pressure in the radial direction, situated at mid-height in the granite cylinders 7 mm from the charge. The gauges were installed in plugs inserted in the specimens. In two of these samples, a PETN charge with a diameter of 8 mm was used, while in the third sample, a pressed TNT charge with a diameter of 10 mm was used. In all three specimens, the gauges both in the axial and radial directions failed too early to give valuable results. To double-check the pressure measurement, two more tests were performed, one specimen with an 8 mm-diameter PETN charge and the other with a 10 mm-diameter pressed TNT charge. Again, the pressure gauges failed to capture valuable pressure signals, probably due to the relative size of the gauge compared to that of the charge diameter. It was decided to proceed to the testing with a pressed TNT charge having a diameter of 20 mm and the pressure gauges positioned only on the axial direction. The pressure gauges were mounted at different distances from the charge to measure shock pressures; four distances were used. PTFE sheets, either 0.3 mm or 0.5 mm in thickness, were used to encapsulate and protect the Manganin pressure gauges; the necessity of using PTFE sheets is discussed later. If several pressure gauges were mounted in one specimen along one axis, the introduction of PTFE cover sheets would inevitably change the shock-wave pressure and distribution along the axis. It was therefore decided to use at most two pressure gauges in each specimen. The configuration of the gauges is given, and the shock reverberation in the PTFE sheets is analyzed in Section 3.

2.4 Specimen design

Three of the ten cylindrical specimens had a diameter (D) of 150 mm and a length (L) of 200 mm, while the seven others were D 240 mm × L 300 mm. The specimens are denoted by "small" and "large" in what follows, as outlined in Fig. 1. Concentric holes were machined out from each end of the specimen, with a 20 mm-diameter hole at one end for inserting the explosive charge and a 50-mm hole at the other end for inserting a specially designed plug equipped with one or two pressure gauges. The granite specimens were manufactured from the same batch of granite, and the outer diameter and inner holes were produced using a lathe. The choice of specimen size was partly motivated by restrictions on size in this machine. Three typical specimen designs and the components for the pressure measurements, including the 50 mm-diameter plug with an embedded pressure gauge, are shown in Fig. 1. Fig. 1a shows a small specimen, i.e., the 150 mm-diameter specimen, while Fig. 1b and 1c show large specimens (D 240 mm), here inserted into a steel tube, which was used to simulate different boundary conditions.

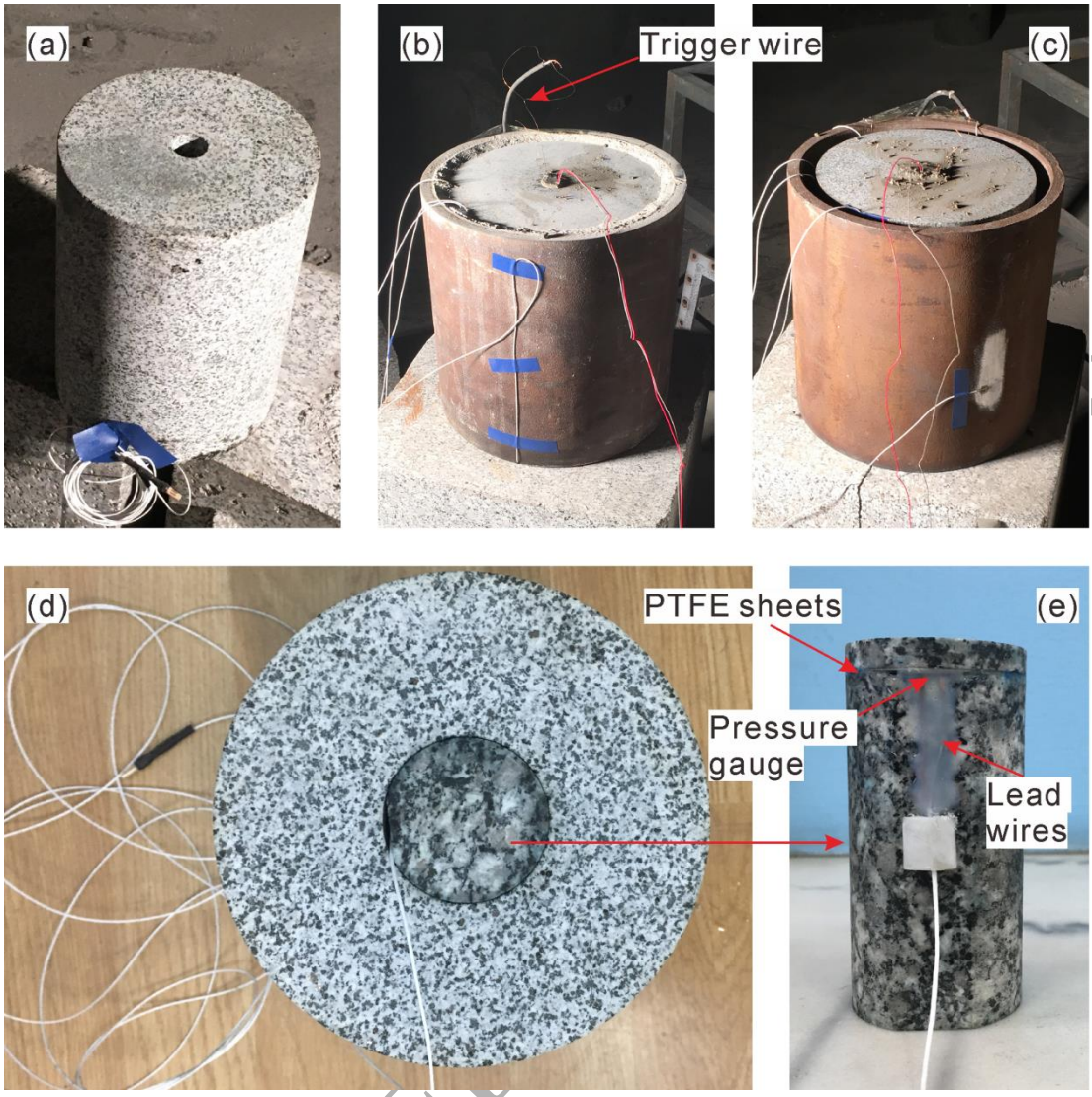

Fig. 1. Specimens and their components: (a) small specimen, D 150 mm; (b) large specimen, D 240 mm, with a confined boundary; (c) large specimen, D 240 mm, without a confined boundary; (d) bottom view of specimen with inserted granite plug; (e) 50 mm insert plug assembled with pressure gauge and granite front plate.

The detailed layout of a large specimen is shown in Fig. 2, with vertical and horizontal cross sections. The diameter of the granite specimen is D, L is the length of the specimen, $D_{borehole}$ and $L_{borehole}$ are the diameter and length of the borehole, respectively, and D_{plug} is the

diameter of the plug for the pressure measurements. The holes for the insert plugs had the same dimensions in all specimens, a diameter of 50 mm and a length of 100 mm.

As shown in Fig. 2, the explosive was placed in the middle of the specimen with the detonator above, and cement grout was used for stemming. The measured dimensions of the specimens and their charge parameters are summarized in Table 1. The diameter of the borehole was chosen based on the results from the pretests, mainly affected by the survivability of the pressure gauges. The steel tube placed outside the specimen had an external diameter of 300 mm (D_{steel}), a wall thickness of 16 mm (t_{steel}), and a length of 300 mm. The steel tube was provided to investigate the effects of radial constraints on the expansion and the fracture pattern of the cylinders. For six of the specimens, a cement grout filled in the gap between the granite and the steel tube, providing a practically confined radial boundary condition. For the four remaining specimens, i.e., the small specimens plus one of the large specimens, the gap was left empty.

In the tests, the boundary condition clearly and significantly influenced the fracture patterns in the specimens. However, from the recorded signals, the Manganin gauges failed before the stress wave had reflected back from the specimen boundary, which means that the actual boundary condition did not influence the recorded pressure history. Accordingly, no separate discussion is given on the effect of specimen boundary upon pressure history.

The 50 mm-diameter insert plug in each specimen was designed to measure the shock-wave pressure in the axial direction of the granite cylinder. To allow measurement of the shock response at different distances from the explosive, the cylindrical plug was assembled from two or three parts consisting of the lower part of the plug (backing cylinder) and either one or two granite discs. Using different thicknesses for these discs allowed the pressure gauge(s) to be positioned at various distances from the explosives. An example of this

arrangement is shown in Fig. 1e, where the approximately 100 mm-long granite plug insert consisted of a 93-mm piece plus a disc with a thickness of 7 mm. Between these pieces is the Manganin pressure gauge protected between two thin PTFE sheets with the active element in the center. The foil with the lead wires of the gauge extends from the circular cross section of the plug and is glued to the side of the plug, as shown in Fig. 1e. In Fig. 1d, the granite of the D 150 mm specimen and the granite of the insert plug have different colors. The reason for this difference is that the remains of lubricant on the granite plug from the assembling operation caused a change in color, even after cleaning with ethanol. The lubricant was necessary to assemble the pressure gauges and the granite plates in a special clamping device (Fig. 4b). The gap between the insert plug and the hole in the specimen had a clearance of 0.25 mm where a common slow cure epoxy with a low viscosity was applied.

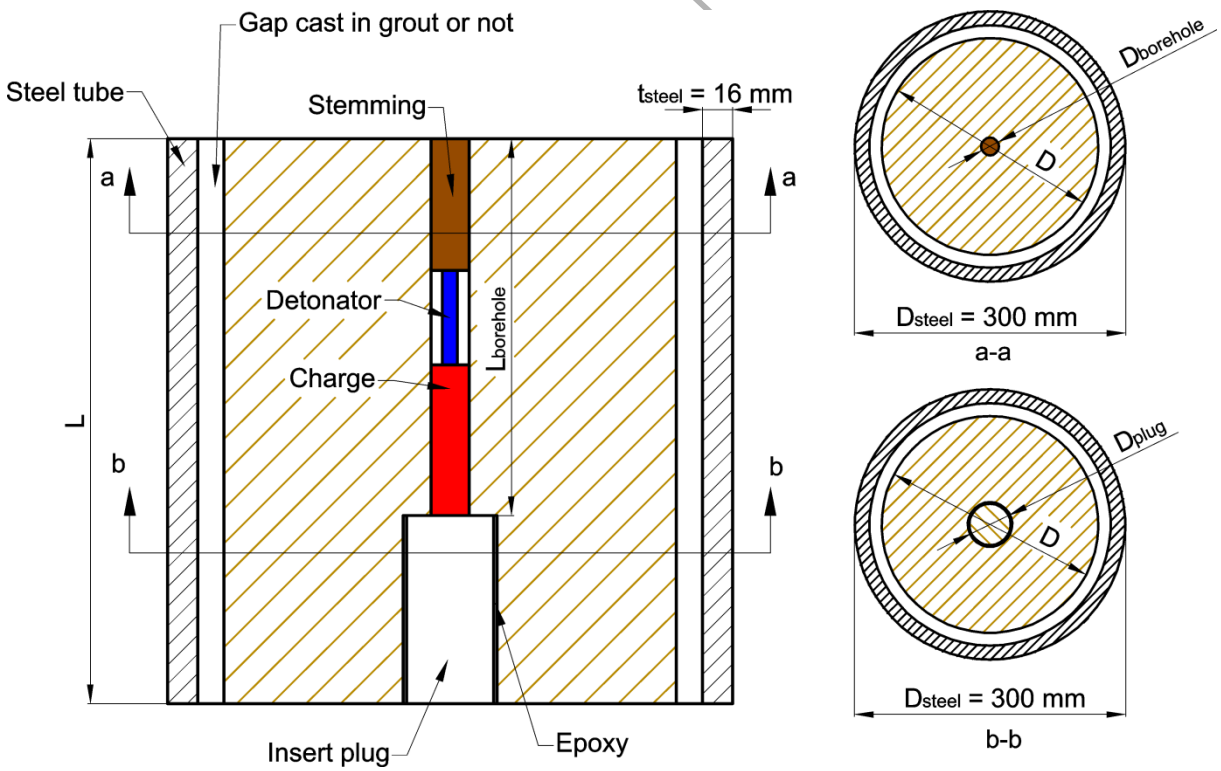

Fig. 2. Cross sections of a large (D = 240 mm) specimen.

Table 1 Charge parameters and dimensions of specimens

Specimen Number	Size of granite specimen $D \times L$ (mm^3)	Borehole $D_{borehole} \times L_{borehole}$ (mm^3)	Charge weight (g)	Density of pressed TNT (g/cm^3)	Charge length (mm)	Boundary condition
1	153.9 × 200.0	20.6 × 98.4	19.83	1.58	39.9	Tube-constrained
2	149.2 × 200.0	20.5 × 94.8	20.49	1.59	41.4	Tube-constrained
3	150.1 × 200.0	20.6 × 100.0	30.16	1.58	59.1	Tube-constrained
4	240.0 × 300.0	20.7 × 200.2	40.10	1.59	79.8	Confined
5	239.8 × 300.0	20.8 × 200.2	39.38	1.59	78.5	Confined
6	239.9 × 299.8	20.6 × 200.3	39.55	1.57	79.5	Confined
7	240.0 × 300.3	20.5 × 200.5	20.02	1.59	40.3	Confined
8	239.8 × 300.2	20.7 × 200.0	40.18	1.59	80.1	Tube-constrained
9	238.0 × 300.0	20.7 × 199.4	40.11	1.59	79.8	Confined
10	228.0 × 300.0	20.5 × 200.0	38.93	1.58	80.0	Confined

3 Pressure measurements

3.1 Configuration of the pressure gauges and charges

The shock pressure measurements were performed using Manganin foil gauges (LM-SS-210AW-048 and LM-SS-210FD-050/SP60) manufactured by Micro-Measurements. The gauges essentially consist of a polymer backing foil with a copper-manganese-nickel alloy conductor strip pattern. The electrical resistivity of the Manganin alloy changes with pressure [10]. The foil gauges were mounted with their pressure-sensitive active element plane directed perpendicular to the propagation direction of the shock wave, which, in impact experiments, is commonly referred to as a longitudinal configuration. The overall dimensions of gauges LM-SS-210AW-048 and LM-SS-210FD-050/SP60 are 44.45×6.35 mm^2 and

$63.5 \times 6.35\ mm^2$, respectively, where both gauges have the same dimensions of $5.33 \times 6.35\ mm^2$ for the active element, but the two gauges have different lengths of lead wires. The longitudinal stress was determined from the Manganin gauge mounted in the longitudinal configuration using a calibration curve [24], which is based on the gauge experiencing a one-dimensional state of straining during shock loading. The calibration curve is widely used in stress measurements with the Manganin gauges in the longitudinal configuration. If the pressure gauge is mounted in other configurations or loaded by a diverging wave, the lateral strain in the gauge itself might contribute to the resistance change. The possible application of pressure foil gauges for measuring a diverging wave was investigated by Charest and Lilly [25] and Gran and Seaman [26], and required a more complex setup with strain gauges mounted together with the pressure sensor. Therefore, the active element of the Manganin gauge was positioned at the centerline of the explosive to produce approximately one-dimensional loading on the gauge. To ensure a stable detonation front, a charge of pressed TNT was employed. The pressed TNT charge was assembled from small pressed TNT cylinders, each with 20 mm-diameter and length, made by compressing TNT powder. The densities of the TNT charges were calculated by measuring their weight and volume, as listed in Table 1. The diameters of the boreholes in the granite cylinders were slightly greater than 20 mm (Table 1), and the average clearance between the pressed TNT charge and the borehole was approximately 0.2 mm. These dimensions ensured a fully coupled charge condition. The layout of the charge was assumed to generate a stable detonation wave.

To improve the survivability of the Manganin pressure gauges and to reduce the piezoelectric effect of quartz in the granite interfering in the signal, thin PTFE sheets were used to encapsulate the pressure gauges. An epoxy (M-bond AE-15 from Micro-Measurements) was used between the PTFE sheets and the Manganin gauge and between the

granite and PTFE sheets in assembling the insert plugs. The layouts of the insert plugs are shown in Fig. 3, while the thicknesses of the granite plates in the plug and the PTFE sheets enclosing the pressure gauge are summarized in Table 2. As seen in Fig. 3, the plug consisted of parts denoted the backing cylinder, middle plate and front plate. Specimens S1, S2, S3 and S10 had only one pressure gauge and thus no middle plate. For the specimens with two pressure gauges, the gauges are denoted the first and secound gauge, the former being closer to the explosive. Due to machining concerns, the thinnest granite front plate was given a thickness of 7 mm. After the two first tests had been conducted, an additional PTFE sheet with a thickness of 0.5 mm was introduced on the top of the front plate for S3, S9 and S10, partly with the intention of capturing a longer time period for the pressure signal. For S6, the entire plug was made from PTFE. The gauges used in the specimens were LM-SS-210AW-048 gauges, with the exception for the first gauges in S4, S5 and S7 where LM-SS-210FD-050/SP60 gauges were used. These gauges had insulation cover and were used without the PTFE sheets in order to examine the necessity of such sheets.

A pressure gauge of type LM-SS-210FD-050/SP60 is shown in Fig. 4a. Fig. 4b shows the assembling of an insert plug (S1-S3) using a clamping fixture with a short hollow steel cylinder to align and keep the granite pieces concentric. A lubricant was applied inside the steel cylinder to avoid sticking to the granite. After assembly, the granite surface was cleaned with ethanol.

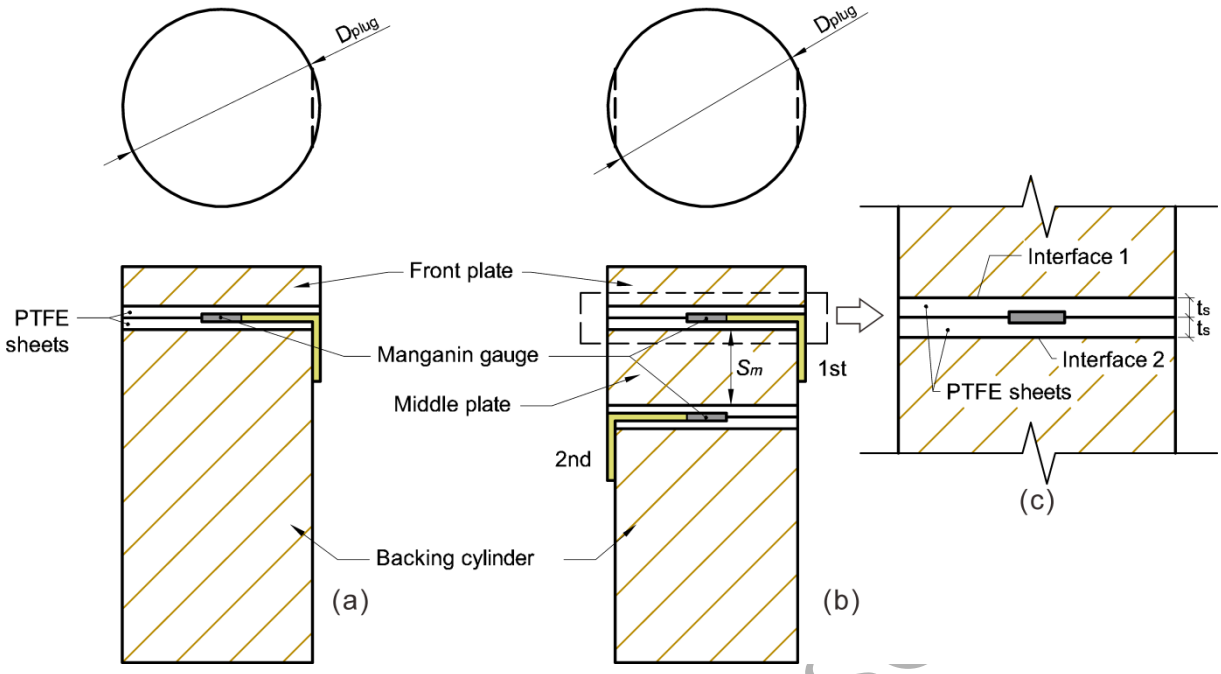

Fig. 3. Schematic configuration of the small cylinder for stress wave measurement: (a) plug with a Manganin gauge enclosed by PTFE sheets between the front plate and the backing cylinder; (b) plug with two Manganin gauges; (c) detail of an embedded gauge.

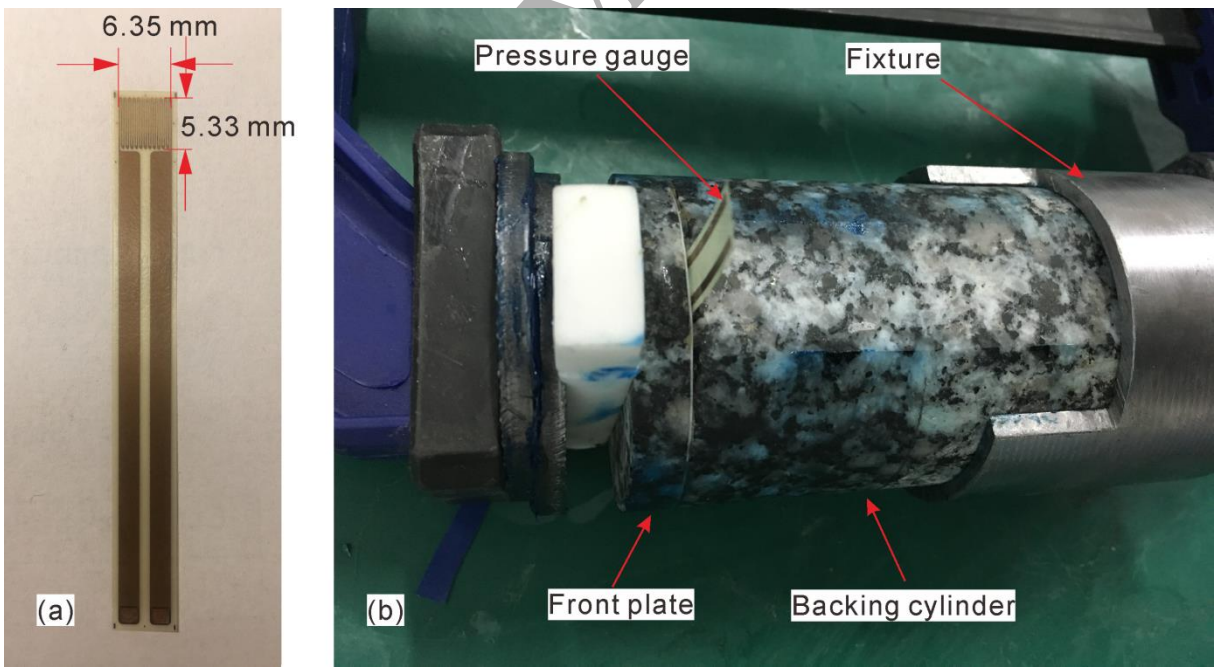

Fig. 4. (a) Manganin gauge (LM-SS-210FD-050/SP60) with its active element and lead wires; (b) gluing of an insert plug (one front plate, one pressure gauge and one backing cylinder) in a fixation clamp.

Table 2 Configurations of insert plugs

Specimen number	Charge weight (g)	Thickness of front plate (mm)	Thickness of middle plate S_m (mm)	Height of backing cylinder (mm)	Thickness of PTFE sheets for the first gauge (mm)	Thickness of PTFE sheets for the second gauge (mm)
1	19.83	6.98	-	93.17	0.3	-
2	20.49	7.04	-	92.95	0.3	-
3*	30.16	6.98	-	93.17	0.5	-
4	40.10	7.00	15.06	78.04	-	0.3
5	39.38	6.89	15.08	78.03	-	0.3
6**	39.55	15.12	30.15	55.28	-	-
7	20.02	15.02	20.11	65.00	-	0.3
8	40.18	6.86	15.08	78.04	0.3	0.3
9*	40.11	15.00	19.94	64.88	0.3	0.3
10*	38.93	10.0	-	90.0	0.5	-

* An additional PTFE sheet with a thickness of 0.5 mm on top of the front plate.

** Insert plug made of PTFE.

3.2 Shock-wave transmission and reflections in the pressure gauge setup

Determining the stresses in the granite from the signals of the embedded Manganin gauge requires an analysis. The user instructions for the Manganin gauges state that the gauges have a nominal response time on the order of nanoseconds. The PTFE sheets and epoxy adhesive surrounding the gauge have an obvious influence on the increase in pressure. A one-

dimensional strain is assumed to occur at the gauge position both in the PTFE sheets and in the granite at the interfaces. To estimate the shock-wave transmission and reflection in the PTFE sheets using the Rankine-Hugoniot relations, the longitudinal stress, σ_x, is assumed to approximate the hydrostatic pressure, p, behind the shock front [13]. The simplified Rankine-Hugoniot conditions, which describe the conservation of the material's mass, momentum and energy, are given by the following [27]:

$$\rho_0 U_S = \rho_1 (U_S - u_p) \quad (1)$$

$$p_1 - p_0 = \rho_0 (U_S - u_0)(u_p - u_0) \quad (2)$$

$$e_1 - e_0 = \frac{1}{2}(p_1 - p_0)(\upsilon_1 - \upsilon_0) \quad (3)$$

Here, the subscripts 0 and 1 refer to the un-shocked and shocked states of the material, respectively, while p, e, υ, ρ, U_S and u_p are the pressure, energy, specific volume, density, shock-wave velocity and particle velocity, respectively.

An additional equation is required to derive the shock Hugoniot state. For most materials, the Hugoniot equation of state can be expressed approximately as a linear relation [27].

$$U_S = C_0 + S u_p \quad (4)$$

Here, C_0 and S are constants, which need to be determined by experiments.

In Eqs. (2) and (3), p_0 is the surrounding pressure (e.g., atmospheric pressure) and can be ignored relative to the high pressure in blasting, and the initial particle velocity u_0 is zero. The Hugoniot data for PTFE and granite are listed in Table 3. Several factors influence the measured Hugoniot data for a given type of rock, such as grain size, microstructure

orientation [14], and porosity [28]. Here, the Hugoniot data (C_0 and S) for the Fangshan granite were assumed similar to those for the granite used by Millett et al. [12], Table 3.

The shock-wave reflection in PTFE sheets was analyzed by the impedance match method, as for instance described by Meyers [27]. The peak pressure from the experiment with S3 was used for the analysis. Fig. 5 explains the method, based on the assumption that a step input of pressure is taken as the initial loading. To calculate the shock states (Points 1 to 4 in Fig. 5), it was assumed that the measured pressure in the gauge was the shock pressure in the granite at the interface with the first sheet and that there was no attenuation of the shock wave in the PTFE sheets. The figure shows the pressure-particle velocity curves (Hugoniot) for the granite and the PTFE, and the isentropic release curve for the granite is assumed to be the reverse of the Hugoniot curve [15,27]. The black and red dashed lines are the shock impedances of the granite and the PTFE, respectively. Point 1 marked on the granite Hugoniot curve corresponds to the initial shock state of the granite near Interface 1 (Fig. 3c). As the shock wave arrives at this interface the shock state changes to Point 2 in the figure, where the granite release curve (orange) intersects with the PTFE Hugoniot curve (red). When the shock wave arrives at the opposite interface, Interface 2 in Fig. 3c, the shock state changes from Point 2 to Point 3, where the PTFE Hugoniot curve (green) intersects with the granite Hugoniot curve (black). The former is the inverse curve for the initial PTFE Hugoniot curve at the pressure of Point 2 and represents the second shock compression of the PTFE. When the shock wave propagates back and reaches Interface 1, the shock state jumps from Point 3 to Point 4, corresponding to the intersection between the PTFE Hugoniot curve (blue) and the granite release curve. The former is the inverse of the PTFE Hugoniot curve (green) at the pressure of Point 3 and is the third shock compression of the PTFE. After one reverberation in the PTFE, the shock state of PTFE (measured by the gauge), Point 4 in the graph, is very close to the initial shock state in the granite, Point 1. Successive reverberations in the PTFE sheets cause the measured shock

pressure to rapidly approach the actual initial pressure in the granite. At Point 1 in Fig. 5 the pressure is 12.58 GPa, while the pressure is 12.55 GPa at Point 4. At this state, we assume that the stress equilibrium in PTFE sheets is reached approximately. Therefore, the pressure determined after one reverberation in the PTFE sheets can be considered to be reasonably close to the pressure in the granite.

Furthermore, for S3, the shock-wave velocity (U_s) in the PTFE corresponding to Point 2 in Fig. 5 has a value of 3.73 mm/μs, determined using Eqs. (1) to (4). Similarly, the shock-wave velocities for Points 3 and 4 are 3.30 mm/μs and 3.34 mm/μs, respectively. Accordingly, the shock wave in one reverberation takes at least 0.59 μs (two sheets of 0.5 mm). For the gauge configuration with PTFE sheets of 0.3 mm, assuming the same pressure, the time becomes 0.35 μs. The time of one full reverberation is regarded as the rise time of the pressure signal. Following the Nyquist theorem, a sampling frequency should be at least twice the bandwidth of the actual signals, which are here approximately 0.6 MHz and 1 MHz for the configurations with PTFE sheets of 0.5 mm and 0.3 mm, respectively. For shock waves with lower magnitudes, the bandwidths of the signals obtained from the gauge configurations are lower. The sampling frequency of 4 MHz used in the tests should thus be sufficient to capture the pressure signals.

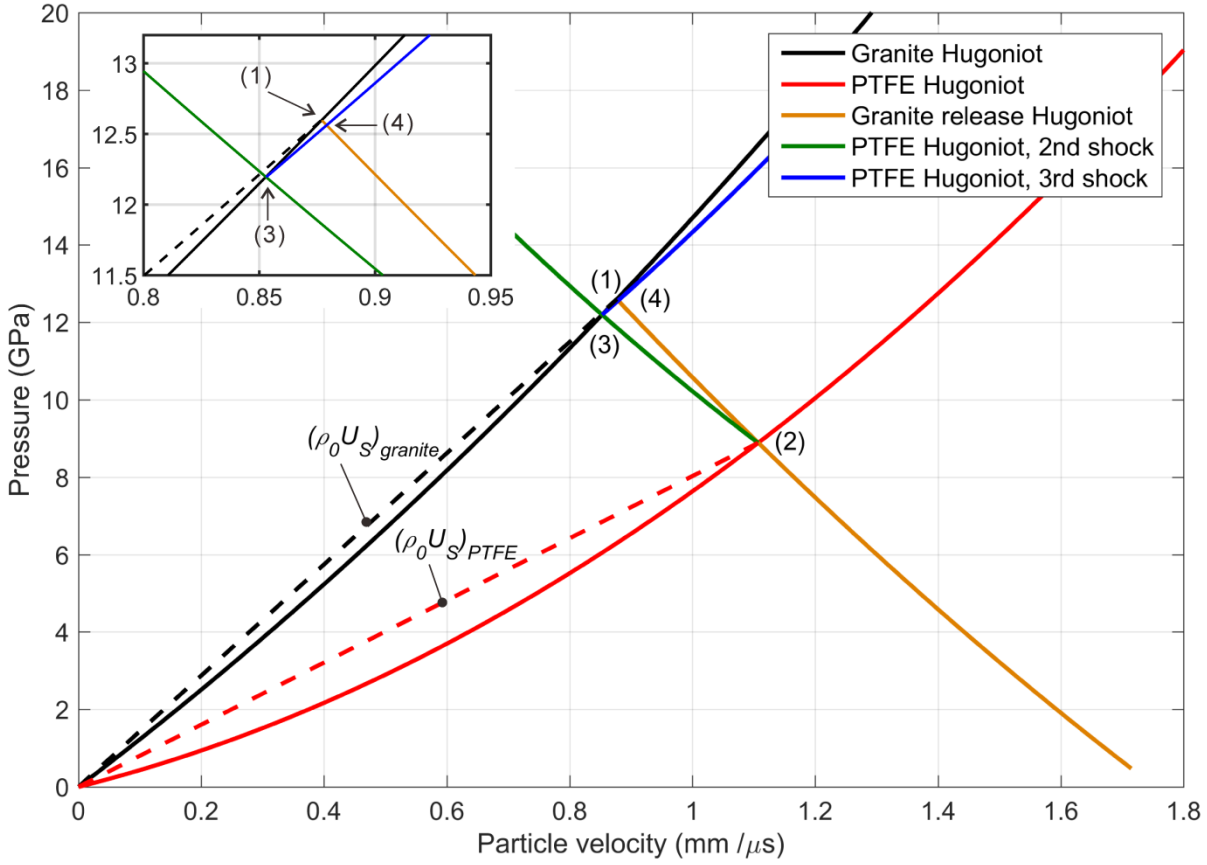

Fig. 5. Pressure-particle velocity space showing the shock-wave reverberation in PTFE sheets for S3; the insert shows an enlarged part of the curves.

Table 3 Physical properties and Hugoniot data for granite and PTFE

Material type	Density (g/cm^3)	Hugoniot, U_S (mm/μs)	Reference
Granite	2.65	U_S = 4.532 + 1.013 μ_P	Millett et al. [12]
PTFE	2.15	U_S = 1.84 + 1.71 μ_P	Meyers [27]

4 Experimental results and analysis

4.1 Measured peak pressure

After carrying out the blast tests as described in Section 2.2, the pressures in each specimen at the monitored positions were determined. Some selected graphs of pressure versus time are

shown in Fig. 6, where the response part of the curves is unfiltered. The trigger moment (detonator initiation) is at 256 μs on the time scale. The gauges in most specimens recorded for approximately 3 μs before they failed and successfully captured the peak pressure; S6 and S10 are exceptions to these results. The recorded peak pressures in all specimens are listed in Table 4 and span from 15.9 GPa at the first gauge to 4.4 GPa at the second gauge.

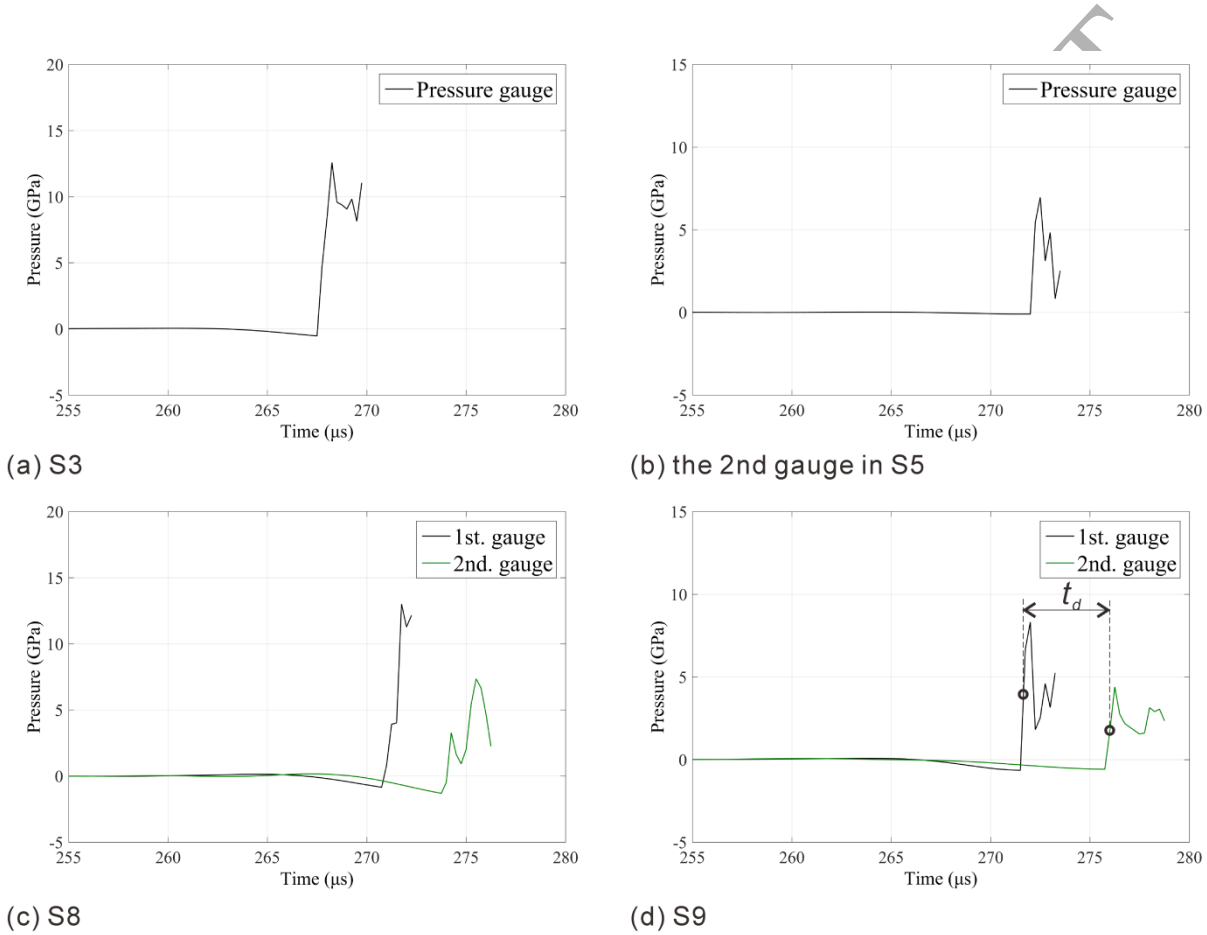

Fig. 6. Pressure traces in different specimens.

Specimens S1 and S2 with charge weights of approximately 20 g and S3 with a charge weight of 30 g had the pressure gauges located at similar distances (7~8 mm, see Table 4) from the explosive. The measured peak pressures in S1 and S2 were 15.9 GPa and 15.8 GPa, respectively, while the peak pressure was 12.6 GPa for S3. One probable reason for the lower pressure in S3 is the extra PTFE sheet located between the charge and the insert plug (Table 2). The measurements of equal peak pressures for the geometrically similar specimens

S1 and S2 indicate a good repeatability of pressure results. The first gauge in both S4 and S5 was not covered by PTFE sheets (Table 2 and Section 3.1) and failed immediately after the shock wave arrived. From the second gauges in specimens S4, S5 and S8, approximately 22 mm from the explosive charge of 40 g, the peak pressures were 9.1 GPa, 7.0GPa and 7.4 GPa, respectively, i.e., quite similar peak pressures that confirm good repeatability. For S7 and S9 with the first gauges at 15 mm from the explosive and with charge weights 20 g and 40 g, the peak pressures were 13.2 GPa and 8.3 GPa, respectively, which was likely an effect of the extra PTFE sheet used on the top of the insert plug of S9 (Table 2) and the effect of omitting PTFE cover sheets for the gauge in S7. The peak pressures measured at the similarly configured second gauge in both of these two specimens were quite similar, 4.9 GPa versus 4.4 GPa. Specimen S8 had its first gauge at 7 mm, similar to S1 and S2, but had twice their charge weight (approx. 40 g vs. 20 g). The peak pressure in S8 reached 13.0 GPa, which is somewhat lower than those for S1 and S2. This result indicates that the weight of the charge does not directly determine the peak pressure.

For specimen S6, where the entire insert plug was made of PTFE, the first gauge failed after 14 μs and before any peak pressure or decreasing pressure was obtained (Fig. 7a). The maximum pressure obtained was 17.8 GPa at a distance of 15.12 mm from the explosive, which is significantly higher than the peak values measured in any of the granite plugs. The second gauge in S6 failed to capture any useful signal due to a setting-up error. In S10, which had a 38.93 g charge, the peak pressure reached only 1.35 GPa at 11.0 mm. The reason for this result was that a deflagration-type event occurred in this specimen, yielding the curve in Fig. 7b. Due to the low pressure in this test, the gauge survived throughout the recording period, i.e., much longer than for gauges in the other specimens.

Table 4 Peak pressures

Specimen	Peak pressure at the first gauge (GPa)	Distance from the explosive to the first gauge (mm)	Peak pressure at the second gauge (GPa)	Distance from the explosive to the second gauge (mm)	Charge weight (g)
1	15.8	7.28	-	-	19.83
2	15.9	7.34	-	-	20.49
3	12.6	7.98	-	-	30.16
4	-	7.00	9.1	22.36	40.10
5	-	6.89	7.0	22.27	39.38
*6	17.8	15.12	-	45.27	39.55
7	13.2	15.02	4.9	35.43	20.02
8	13.0	7.16	7.4	22.84	40.18
9	8.3	15.8	4.4	36.34	40.11
10	1.35	11.0	-	-	38.93

* Insert plug made of PTFE.

The ten specimens had explosive charges with similar density and diameter, so it is reasonable to assume that the detonations were stable and provided a constant Chapman-Jouguet (CJ) pressure (S10 is an exception). According to the experiments by Kennedy [29], for plates driven by an explosion, there exists a maximum length of the explosive that contributes to the acceleration of the plate to a critical velocity, and this velocity cannot be increased only by increasing the length of the explosive. Using the 60 degree cone model of Kennedy [29] for the charge of the present specimens, a charge length longer than 18 mm would not significantly increase the peak pressure. The small difference in peak pressures between specimens with 20 g and 40 g charges is thus not surprising. However, the results in Table 4 clearly show that the distance from the charge is an essential parameter for the pressures.

4.2 Rise time of pressure histories

The pressures measured by the gauges with PTFE sheets in the specimens increased to the peak values within a time period of 0.5 μs, as shown in some of the graphs in Fig. 6. After the peak in the pressure, the gauges failed within a few microseconds. For the pressure gauges without PTFE sheets, the first gauge in S4 and S5 failed immediately after the shock wave arrived, while the first gauge in S7 indicated a significant rise within 0.25 μs, which was the sampling interval. The exceptions were S6 (plug of PTFE) and S10, as shown in Fig. 7, where the first gauge in S6 revealed a 14-μs rise time to obtain the maximum pressure and the gauge in S10 had a rise time of 16 μs. During the rise time of S6 (Fig. 7a), the pressure curve displays an initial step with a 2.5 GPa pressure increase in the first 0.5 μs, followed by a nearly linear development of the curve until the maximum pressure. The increasing part of the curve for this specimen agrees with the response of thermoplastic materials subjected to nonlinear viscoelastic shock waves in general, as outlined by Wang [30]. The shock response of PTFE materials reported in the literature is complex, where the shocked material is considered a three-phase mixture of one amorphous and two crystalline phases [31,32]. Resnyansky et al. [32] concluded that the phase transition caused by a shock wave could result in a broadening front during wave propagation. This process may explain the observation of a significantly longer rise time for S6 than for the others.

Vantine et al. [33] embedded Manganin gauges directly in the explosive to measure the pressures and found that a 0.25 mm-thick PTFE sheet encapsulation of their Manganin gauges did not significantly perturb the pressure development. Moreover, Bourne et al. [31] conducted impact experiments on PTFE plates, measured the longitudinal stresses with embedded Manganin gauges, and obtained an increase (approximately 0.2 μs) to 0.9 GPa at a distance of 5 mm from the impacted surface. In conclusion, taking into account also the result

of S6, the use of PTFE materials with thicknesses greater than a few millimeters in connection with pressure gauge configurations should be avoided.

Some other issues should be mentioned. The rise time for S10 was approximately 16 μs, which was longer than that for the other specimens. In addition, the post-blast specimen (S10) did not have visible fractures on the top surface or major damage in the cross section close to the bottom of the borehole. The peak pressure, rise time and fracture pattern clearly indicated that the pressed TNT charge deflagrated in this test. For S8, the pressure arrived at the maximum value after a small step, visible in Fig. 6c. A possible reason for the step is that the pressure gauges or sheets were not properly attached in the insert plug, resulting in gauge vibration during the shock-wave reverberation.

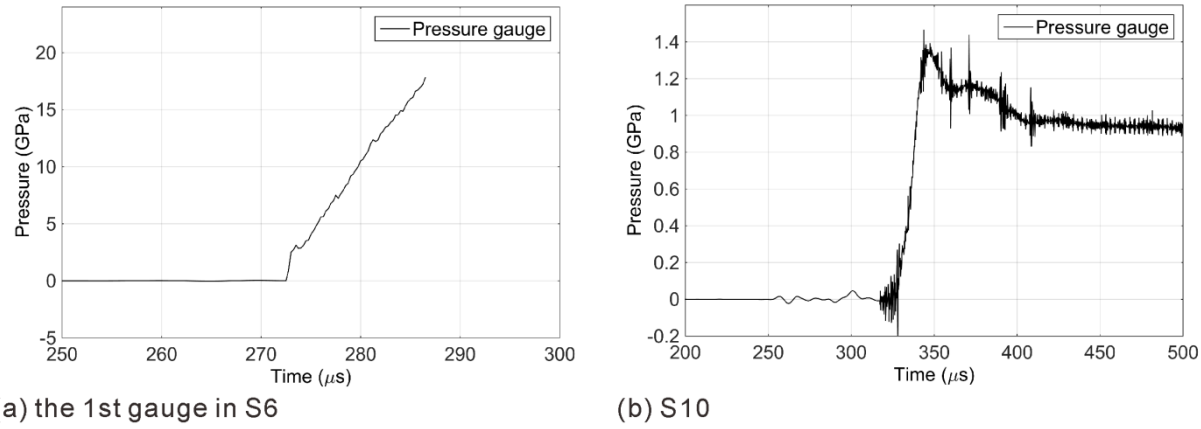

Fig. 7. Pressure traces of two experiments different to all the others.

4.3 Shock-wave velocity

From the pairs of pressure gauges in some specimens, the shock-wave velocity in the rock may be determined. With the 0.5-μs rise time on the pressure curves (Section 4.2), the arrival time of the shock wave at the gauges was taken equal to half of the rise time. The times for shock-wave propagation through the PTFE sheets were accounted for. Using S9 as a reference, the delay time between the two gauges, t_d noted in Fig. 6d, was approximately 4.3 μs. Then,

the average velocity, U, of the shock-wave propagation through the middle granite plate (thickness S_m, Fig. 3b) can be calculated from the following:

$$U = \frac{S_m}{t_g} \quad (5)$$

$$t_g = t_d - t_{p1} - t_{p2} \quad (6)$$

Here, t_g is the time for the shock wave to propagate through the middle granite plate, t_{p1} is the travel time for the shock wave to propagate through one PTFE sheet at the first gauge, and t_{p2} is the travel time through one sheet for the second gauge. Times t_{p1} and t_{p2} are determined by dividing the relevant sheet thickness by the shock-wave velocity, which can be calculated from the Hugoniot equation for PTFE at the corresponding peak pressures. In addition, for the specimens (S4, S5 and S7) in which the first pressure gauge was not enclosed by PTFE sheets, the shock-wave velocity was determined from the arrival time at the first gauge and the defined arrival time at the second gauge (Fig. 6d). The resulting velocities for the specimens that allowed this calculation are given in Table 5. Specimen S6 is not included as its insert plug was composed of PTFE.

Table 5 Average velocity of the shock wave through the middle plate of the granite

Specimen number	Average velocity of shock wave (mm/μs)	Thickness of front plate (mm)	Thickness of middle plate (mm)
S4	5.18	7.00	15.06
S5	5.20	6.89	15.08
S7	4.58	15.02	20.11
S8	5.34	6.86	15.08
S9	4.93	15.00	19.94

As seen from Table 5, for specimens S4, S5 and S8, in which the front plate was approximately 7 mm thick, the calculated average velocities through the middle plate range from 5.18 mm/μs to 5.34 mm/μs. For S7 and S9, which had approximately 15 mm-thick front plates, the calculated velocities are 4.58 mm/μs and 4.93 mm/μs, respectively. Obviously, the thickness of the front plates also determines the distance to the explosive. The observed shock-wave velocities in the table are all higher than the compressional elastic wave velocity (4.0 mm/μs to 4.4 mm/μs) in the granite.

4.4 Shock-wave attenuation

The measured peak pressures at the various gauge locations were used to describe the shock-wave attenuation in the granite. The relation between the peak pressure, *p*, and the travel distance, *x*, from the explosive has been expressed by an empirical experimental relation [34]:

$$p = A \cdot \exp(-b \cdot x) \tag{7}$$

Here, *A* and *b* are constants. The constant *A* depends on the initial shock loading on the borehole wall, while *b* is the attenuation factor for the material. For granite, the constant *b* is considered an intrinsic property; for instance, for Lithonia granite, *b* was found to be 0.018 (1/mm) [34]. Klee et al. [35] used the exponential relation to describe the shock attenuation with distance in Cu, Al and PMMA. Banadaki [36] used a very similar power equation for pressures measured in the radial direction in a granite.

Fig. 8 shows a plot of the peak pressures versus the distances from the explosive as measured in the tests on specimens S1 - S5 and S7 - S9, together with three curves based on a fit by applying Eq. (7). The black curve is the result of the fit using the peak pressures of all these specimens. Specimens S6 and S10 are excluded as the former had the PTFE plug and the latter the charge deflagration. The fitted constants *A* and *b* for the black curve are 19.4 GPa and 0.040, respectively, with the corresponding coefficient of determination (R-

square) equal to 0.87. The shock attenuation is mainly dependent on granite damage and fracture, the release wave immediately behind the shock pressure in the detonating explosive, and geometrical spreading in the granite. Since the gauges were located close to the explosive in the axis of the cylinder, we may assume that the geometrical attenuation in the axial direction made a limited contribution to the entire attenuation.

The peak pressure obtained from the first gauge in S7, located approximately 15 mm from the explosive, is significantly higher than the corresponding pressure predicted by the fitted curve (Fig. 8). One reason might be that there were no PTFE sheets covering the pressure gauge in this specimen, and this may have caused some uneven contact and affected the pressure. A significant oscillation with several peaks in the rise part of the pressure curve for this specimen supports this. The most important observation in Fig. 8 is that the data scatter from the fitted curve decreases with increasing distance from the explosive.

By considering specimens S3 and S9 separately, in both of which a 0.5 mm-thick PTFE sheet was placed between the charge and the insert plug, the three peak pressures recorded for these specimens were used to fit the green curve in Fig. 8. The curve is clearly situated below the black curve. A third fit, shown with the red curve in the figure, is the result obtained using the remaining peak pressure data (excluding the first gauge in S7). The green and red curves are basically parallel and have attenuation factors (b) of 0.0396 and 0.0414, respectively, i.e., similar values. The pressure constants A for the curves are 16.8 GPa and 20.1 GPa, respectively, i.e., a higher value for the red curve. The shock impedance of the pressed TNT was higher than that of PTFE but lower than that of the granite, which may have caused the loads (initial pressure) on the top surfaces of the granite plugs in S3 and S9 (green curve) to become lower than those for the specimens that had insert plugs in direct contact with the TNT. As seen in Fig. 8, the green curve corresponds to a reduction of 11-15% in the shock pressure.

For a given case, the constant *A* may take other values, as it is determined by the initial load conditions, such as type of explosive, borehole and charge diameters, etc. The determined attenuation factor (approximately 0.04), however, is more likely a combined result of the properties of the tested granite and the explosive (with its rate of release behind the detonation wave), valid for the investigated pressure range and distance from the charge (respectively 16 GPa to 4 GPa and 0 mm to 40 mm ($2 \cdot D_{borehole}$)).

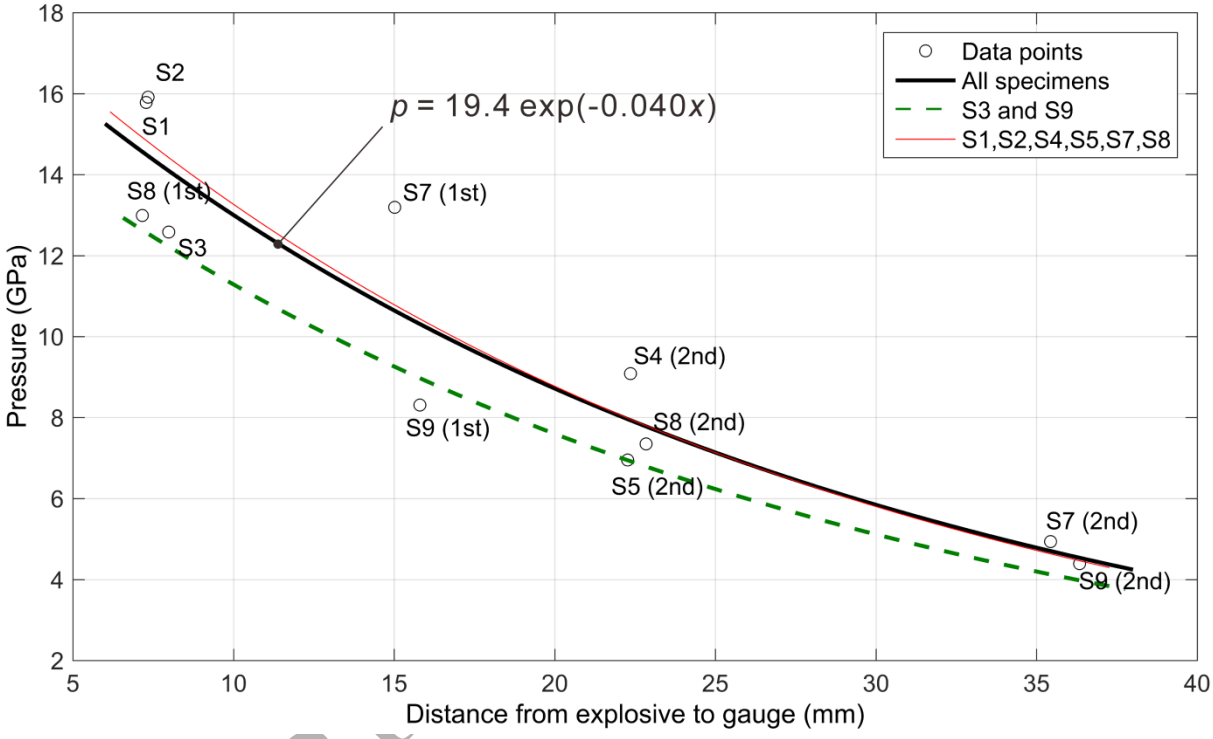

Fig. 8. Summary and fitted curves of the peak pressure in granite.

5 Discussion

5.1 Comparison of measured pressure with CJ pressure

Specimen S6 with the insert plug made entirely of PTFE allows an evaluation of the detonation wave loading at the interface at the bottom of the borehole. The shock impedance of the pressed TNT was higher than that of the PTFE; thus, a shock wave was transmitted into

the PTFE and a release wave reflected into the detonation products. The CJ pressure, p_j, is estimated by the following equation from CJ theory [27]:

$$p_j = \frac{\rho_{TNT} VOD^2}{\gamma + 1} \tag{8}$$

Here, *VOD* is the velocity of detonation, ρ_{TNT} is the initial density of TNT, and γ is the polytropic gas constant.

The shock pressure at the interface with the PTFE can be estimated by assuming that the behavior of the detonation products can be treated as the isentropic expansion of an ideal gas, where the particle velocity at the interface can be expressed by the following [37]:

$$u_x = \frac{VOD}{\gamma + 1}\left\{1 + \frac{2\gamma}{\gamma - 1}\left[1 - \left(\frac{p_x}{p_j}\right)^{\frac{\gamma-1}{2\gamma}}\right]\right\} \tag{9}$$

Here, p_x is the pressure at the interface. Due to the pressed TNT density of 1.57 g/cm^3, the gas constant γ is set equal to 2.85 as suggested by Lee et al. [38], and *VOD* is equal to 6.8 mm/μs [37].

The PTFE shock Hugoniot equation at the interface may be derived by combining Eqs. (2) and (4) and yields the following:

$$p_x = \rho_0 \left(C_0 + S u_x\right) u_x \tag{10}$$

Here, the corresponding parameters for PTFE are used, as listed in Table 3. Combining Eqs. (8) to (10) gives an implicit equation system for determining the CJ pressure, the pressure at the interface and the particle velocity. The obtained values for the CJ pressure and the interface pressure are 18.9 GPa and 18.7 GPa, respectively. In specimen S6, the observed

maximum pressure at a distance of 15.12 mm from the explosive was 17.8 GPa, i.e., a decrease of 0.9 GPa over the distance.

For the other specimens, as the shock impedance of the granite was higher than that of PTFE, the unknown pressure in the granite at the explosive-to-granite interface should theoretically have been higher than the pressure (18.7 GPa) at the explosive-to-PTFE interface under the same loading condition. In the granite plugs, the measured peak pressures (S7 and S9) at 15 mm from the explosive were significantly lower than the pressure measured at the same distance in the PTFE plug in S6 (Table 4). Assuming that the same CJ pressures were achieved in all specimens (except S10), this result indicates faster attenuation in granite than in PTFE. Accordingly, although the use of the PTFE sheets favors survivability of the pressure gauges, the relative difference in damping between the materials should be considered, for instance when designing experiments with rock and where thicker plates of PTFE are applied.

Moreover, the maximum of the peak pressures measured in the granite insert plugs was approximately 16 GPa at a distance of 7 mm, 2.9 GPa below the CJ pressure, which shows the effects of the shock-wave transmission at the interface and the attenuation through the 7 mm.

5.2 Post-blast specimens

The long rise time and the low peak pressure for S10 implied that the charge in this specimen deflagrated. The measured peak pressure was 1.35 GPa at a distance of 11.0 mm from the explosive (Table 4), and the rise time was approximately 16 μs (Fig. 7b). To illustrate the differences in the fractures around the boreholes caused by detonation as opposed to deflagration, S5 was chosen for comparison. For S5, the peak pressure was 7.0 GPa at a distance of approximately 22 mm from the explosive, and the rise time was approximately 0.5 μs (Fig. 6b).

In the tests, S5 and S10 were confined by the steel tube and the cement grout in the gap. Approximately 10% of specimen S5 was blasted away from the top of the cylinder. The post-blast boreholes were filled with a mixture of epoxy and fluorescent green powder. After the epoxy had cured, the steel tubes with the specimens were cut horizontally to obtain the cross section normal to the borehole at approximately 10 mm from its bottom (110 mm from the specimen bottom). When granite cylinder S5 was removed from the steel tube, the granite fell apart into many pieces. One piece included a part of the post-blast borehole with the epoxy mixture. This piece is shown in Fig. 9a, where the initial 20 mm-diameter borehole had expanded to a final "equivalent" diameter of 47 mm. The granite of post-blast specimen S10 was approximately intact (Fig. 9b) and displayed practically no borehole expansion, but three clear cracks radiated from the borehole. The limited damage to S10 supports the conclusion of charge deflagration.

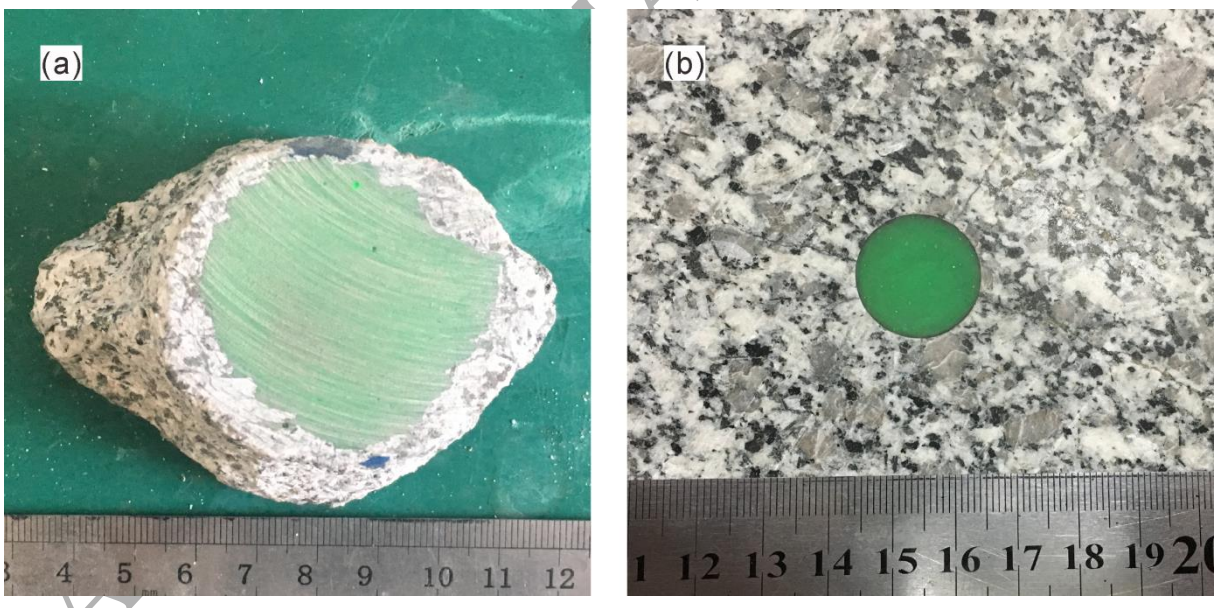

Fig. 9. Post-blast specimens: (a) one fragment from S5 showing post-blast borehole; (b) cross section of S10 showing post-blast borehole.

5.3 Pressure trace variations and gauge survivability

Specimen S10 in which the charge deflagrated showed obvious differences in the measured pressure trace compared to the other specimens with granite plugs. These differences include the magnitude of the peak pressure in the granite, the rise time and the surviving of the gauge. The peak pressure is commonly known to depend mainly on the chemical reaction of the TNT charge. The slow rise time for S10 may be due to two reasons. First, a deflagration has a slower chemical reaction rate than a detonation does. Fourney et al. [2] measured the borehole pressure in PMMA blocks and found that the rise times caused by detonation and deflagration of charges were 3.5 μs and 100 μs, respectively. The second reason is connected to the microstructure of the granite. Kirk [14] observed, in impact experiments on Gosford sandstone, pressures of approximately 1 GPa and 2.5 GPa with rise times of 3 μs and less than 1 μs, respectively. He argued that at low pressure, the granular material structure results in a roughened shock-wave front arriving at the gauge at different times, i.e., causing an uneven pressure over the gauge area and thereby a longer rise time.

In specimen S10, the pressure gauge survived for a longer period than did those in the other specimens. The low pressure, 1.35 GPa, is the probable reason for this result. For gauge survivability, Ginsberg and Asay [8] stated that the heterogeneity of the material is the greatest problem when using foil Manganin gauges. Subjected to shock pressures of the same order, the gauge embedded in the PTFE plug (homogeneous) in specimen S6 survived 14 μs longer than did the gauges embedded in the granite insert plugs in the other specimens.

6 Conclusions

The near-field response of granite to blasting has been investigated, and the results from tests on ten cylindrical specimens are analyzed. Although the test program includes few repetitions of specimens and gauge configurations, the test results allow satisfactory confidence about

general trends observed during this study. The investigation has led to the following conclusions:

1. The pressures caused by detonated TNT charges in granite were measured by means of Manganin gauges located at distances of 7, 15, 22 or 35 mm from the explosive along the cylinder axis. The peak pressures varied from 15.9 GPa to 4.4 GPa depending on the distance from the explosive. The peak pressure measured for the specimen that experienced charge deflagration was 1.35 GPa at a distance of 11.0 mm from the explosive.

2. At a similar distance from the charge (22 mm) and for similar specimen geometry, the peak pressure in three specimens varied from 7.0 GPa to 9.1 GPa.

3. The repeatability of the peak pressure for similar specimens was quite good. For the two specimens S1 and S2 the measured values were 15.9 GPa and 15.8 GPa.

4. The rise time for the measured peak pressures in the granite caused by the TNT detonations was fast (approximately 0.5 μs for the gauges with PTFE sheets), while the rise time for the peak pressure due to deflagration was much longer (16 μs).

5. The average travel velocity of the shock wave in the granite was determined from the distance and the travel time of the shock-wave front between pairs of adjacent gauges. The measured velocities ranged noticeably from 5.34 mm/μs to 4.58 mm/μs, mainly depending on the distance from the explosive.

6. By assuming an exponential relation between the peak pressure in the granite and the distance from the explosive, curves were fitted to the experimental results. The peak pressure (GPa) could be expressed as a function of the distance (mm) with the formula $p = A \cdot \exp(-0.04x)$. Here, A was related to the initial pressure at the borehole bottom and

ranged from 16.8 GPa to 20.1 GPa for the fitted curves, with a value of 19.4 GPa when considering all specimens.

7. The pressure attenuated more slowly in pure PTFE; therefore, the use of thicker PTFE sheets for the protection of pressure gauges in similar studies should be considered carefully.

Acknowledgments

This work is financed by the University Centre in Svalbard. The authors wish to thank Mr. He C.L., Mr. Cheng Z.Y., Mr. Zhou Z.S. and Mr. Feng of the Beijing Institute of Technology for the support in conducting the experiments in the State Key Laboratory of Explosion Science and Technology. The authors also thank the reviewers for their valuable comments and suggestions.

References

[1] Fourney WL, Barker DB, Holloway DC. Model studies of explosive well stimulation techniques. Int J Rock Mech Min Sci Geomech Abstr 1981;18:113–27. doi:10.1016/0148-9062(81)90737-3.

[2] Fourney WL, Barker DB, Holloway DC. Model studies of well stimulation using propellant charges. Int J Rock Mech Min Sci Geomech Abstr 1983;20:91–101. doi:10.1016/0148-9062(83)90330-3.

[3] Nie S. Measurement of borehole pressure history in blast holes in rock blocks. Proc. 6th Int. Symp. Rock Fragm. by Blasting, Johannesburg, South Africa: South African Institute of Mining and Metallurgy; 1999, p. 91–7.

[4] Mencacci S, Chavez R. The measurement and analysis of detonation pressure during blasting. Brighton Conf. Proceedings, Eur. Fed. Explos. Eng., 2005, p. 231–6.

[5] Banadaki MMD, Mohanty B. Numerical simulation of stress wave induced fractures in rock. Int J Impact Eng 2012;40–41:16–25. doi:10.1016/j.ijimpeng.2011.08.010.

[6] Davies F, Smith E, De La Cruz C. The measurement of detonation waves in composite explosives. Proceeding 13th Anaual Symp. Explos. Blasting Res., Las Vegas, Nevada: International Society of

Explosives Engineers; 1997, p. 145–59.

[7] Taylor NE, Braithwaite CH, Morley MJ, Chapman DJ, Proud WG. Explosive-rock interactions; experimental study. AIP Conf. Proc., vol. 1195, 2009, p. 1139–42. doi:10.1063/1.3295003.

[8] Ginsberg MJ, Asay BW. Commercial carbon composition resistors as dynamic stress gauges in difficult environments. Rev Sci Instrum 1991;62:2218–27. doi:10.1063/1.1142340.

[9] Rosenberg Z, Ginzburg A, Ashuach Y. More on commercial carbon resistors as low pressure gauges. Int J Impact Eng 2007;34:732–42. doi:10.1016/j.ijimpeng.2006.02.006.

[10] Bourne N. Materials in mechanical extremes: fundamentals and applications. Cambridge University Press; 2013.

[11] Rosenberg Z, Ginzberg A, Dekel E. High shock pressure measurements using commercial manganin gauges. Int J Impact Eng 2009;36:1365–70. doi:10.1016/j.ijimpeng.2009.03.012.

[12] Millett JCF, Tsembelis K, Bourne NK. Longitudinal and lateral stress measurements in shock-loaded gabbro and granite. J Appl Phys 2000;87:3678–82. doi:10.1063/1.372399.

[13] Willmott GR, Proud WG. The shock Hugoniot of Tuffisitic Kimberlite Breccia. Int J Rock Mech Min Sci 2007;44:228–37. doi:10.1016/j.ijrmms.2006.07.006.

[14] Kirk S. Shock compression and dynamic fragmentation of geological materials. PhD Thesis, University of Cambridge, 2014.

[15] Zhang QB, Braithwaite CH, Zhao J. Hugoniot equation of state of rock materials under shock compression. Philos Trans R Soc A Math Phys Eng Sci 2017;375:20160169. doi:10.1098/rsta.2016.0169.

[16] Haas CJ, Rinehart JS. Coupling between unconfined cylindrical explosive charges and rock. Int J Rock Mech Min Sci 1965;2:13–24. doi:10.1016/0148-9062(65)90019-7.

[17] Petersen CF, Murri WJ, Cowperthwaite M. Hugoniot and release-adiabat measurements for selected geologic materials. J Geophys Res 1970;75:2063. doi:10.1029/JB075i011p02063.

[18] Nakazawa S, Watanabe S, Iijima Y, Kato M. Experimental investigation of shock wave attenuation in basalt. Icarus 2002;156:539–50. doi:10.1006/icar.2001.6729.

[19] Tilert D, Svedbjörk G, Ouchterlony F, Nilsson B, Temun A, Mattsson L. Measurement of explosively induced movement and spalling of granite model blocks. Int J Impact Eng 2007;34:1936–52. doi:10.1016/j.ijimpeng.2006.11.006.

[20] Tan S, Wang C, Shu CW, Ning J. Efficient implementation of high order inverse Lax-Wendroff boundary treatment for conservation laws. J Comput Phys 2012;231:2510–27. doi:10.1016/j.jcp.2011.11.037.

[21] Wang C, Ding J, Tan S, Han W. High Order Numerical Simulation of Detonation Wave Propagation Through Complex Obstacles with the Inverse Lax-Wendroff Treatment. Commun Comput Phys 2015;18:1264–81. doi:10.4208/cicp.160115.150915a.

[22] Yan P, Zhou W, Lu W, Chen M, Zhou C. Simulation of bench blasting considering fragmentation size distribution. Int J Impact Eng 2016;90:132–45. doi:10.1016/j.ijimpeng.2015.11.015.

[23] Chi LY, Zhang ZX, Aalberg A, Yang J, Li. Charlie Chunlin. Fracture processes in granite blocks under blast loading. Rock Mech Rock Eng 2018. doi:10.1007/s00603-018-1620-0.

[24] Rosenberg Z, Moshel G. Revisiting the calibration of manganin gauges for lateral stress measurements in shock-loaded solids. J Appl Phys 2014;115. doi:10.1063/1.4868296.

[25] Charest JA, Lilly MD. PFV2 stress gauges for non-planar wave applications. Part I. AIP Conf. Proc., vol. 309, AIP; 1994, p. 1731–4.

[26] Gran JK, Seaman L. Analysis of piezoresistance gauges for stress in divergent flow fields. J Eng Mech 1997;123:36–44.

[27] Meyers MA. Dynamic behavior of materials. John wiley & sons; 1994.

[28] Hoerth T, Bagusat F, Hiermaier S. Hugoniot data of Seeberger sandstone up to 7 GPa. Int J Impact Eng 2017;99:122–30. doi:10.1016/j.ijimpeng.2016.08.003.

[29] Kennedy JE. Behavior and Utilization of Explosives in Engineering Design. 12th Ann. Symp., ASME, Albuquerque, NM, 1972.

[30] Wang L. Foundations of stress waves. Elsevier; 2011.

[31] Bourne NK, Millett JCF, Brown EN, Gray GT. Effect of halogenation on the shock properties of semicrystalline thermoplastics. J Appl Phys 2007;102. doi:10.1063/1.2778746.

[32] Resnyansky AD, Bourne NK, Millett JCF, Brown EN. Constitutive modeling of shock response of polytetrafluoroethylene. J Appl Phys 2011;110:033530. doi:10.1063/1.3619804.

[33] Vantine H, Chan J, Erickson L, Janzen J, Weingart R, Lee R. Precision stress measurements in severe shock-wave environments with low-impedance manganin gauges. Rev Sci Instrum 1980;51:116–22.

doi:10.1063/1.1136038.

[34] Hustrulid WA. Blasting principles for open pit mining: general design concepts. Balkema; 1999.

[35] Klee C, Kroh M, Ludwig D. Experiments on the attenuation of shock waves in condensed matter. AIP Conf. Proc., vol. 78, AIP; 1982, p. 486–90.

[36] Banadaki MMD. Stress-wave induced fracture in rock due to explosive action. PhD Thesis, University of Toronto, 2010.

[37] Zhang BP, Zhang QM, Huang FL. Detonation physics. Arms Industry Press (In Chinese); 2006.

[38] Lee EL, Hornig HC, Kury JW. Adiabatic Expansion Of High Explosive Detonation Products, Lawernce Livermore Report UCRL-50422. Livermore, CA (United States): 1968. doi:10.2172/4783904.